BIOCHEMISTRY
including biophysical chemistry & molecular biology

Article

pubs.acs.org/biochemistry

Stoichiometry of the Calcineurin Regulatory Domain−Calmodulin Complex

Tori B. Dunlap,[†] Hou-Fu Guo,[†] Erik C. Cook,[†] Emily Holbrook,[†] Julie Rumi-Masante,[†] Terrence E. Lester,[†] Christopher L. Colbert,[‡] Craig W. Vander Kooi,[†] and Trevor P. Creamer*[,†]

[†]Center for Structural Biology, Department of Molecular and Cellular Biochemistry, University of Kentucky, 741 South Limestone Street, Lexington, Kentucky 40536-0509, United States

[‡]Department of Chemistry and Biochemistry, North Dakota State University, P.O. Box 6050, Department 2710, Fargo, North Dakota 58102-6050, United States

Supporting Information

ABSTRACT: Calcineurin is an essential serine/threonine phosphatase that plays vital roles in neuronal development and function, heart growth, and immune system activation. Calcineurin is unique in that it is the only phosphatase known to be activated by calmodulin in response to increasing intracellular calcium concentrations. Calcium-loaded calmodulin binds to the regulatory domain of calcineurin, resulting in a conformational change that removes an autoinhibitory domain from the active site of the phosphatase. We have determined a 1.95 Å crystal structure of calmodulin bound to a peptide corresponding to its binding region from calcineurin. In contrast to previous structures of this complex, our structure has a stoichiometry of 1:1 and has the canonical collapsed, wraparound conformation observed for many calmodulin−substrate complexes. In addition, we have used size-exclusion chromatography and time-resolved fluorescence to probe the stoichiometry of binding of calmodulin to a construct corresponding to almost the entire regulatory domain from calcineurin, again finding a 1:1 complex. Taken in sum, our data strongly suggest that a single calmodulin protein is necessary and sufficient to bind to and activate each calcineurin enzyme.

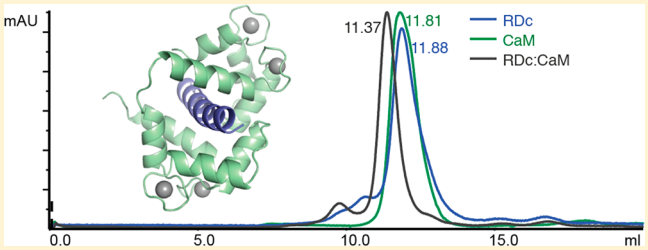

Calcineurin (CaN) is a calcium/calmodulin (CaM)-activated serine/threonine phosphatase. It was originally identified by Wang and Desai,[1] Watterson and Vanaman,[2] and Klee and Krinks[3] as an inhibitor of the CaM-activated cyclic 3′,5′-nucleotide phosphodiesterase. These groups demonstrated that CaN binds to, and thereby depletes, CaM in brain tissue, preventing activation of cyclic 3′,5′-nucleotide phosphodiesterase by CaM.

Since its discovery, CaN has been shown to play roles in cardiac, vasculature, and nervous system development.[4] CaN signaling is also necessary for learning and memory, skeletal muscle growth, and immune system activation.[4] Because of its roles in these varied signaling systems, inappropriate CaN regulation has been implicated in a number of pathological states, including Alzheimer's disease,[5,6] Down syndrome,[7] and cardiac hypertrophy.[8,9] Additionally, CaN's ability to dephosphorylate, and thereby activate, the nuclear factor of activated T-cells (NFAT) family of transcription factors makes it the target of the immunosuppressant drugs FK506 and cyclosporin A.[4,10]

CaN is a heterodimer composed of a 57−61 kDa A chain (CnA) and a 19 kDa B chain (CnB). CnA is composed of the catalytic domain, CnB binding helix, regulatory domain (RD), autoinhibitory domain (AID), and C-terminal tail (CT) (Figure 1).[11] CnB is a calcium binding EF hand protein that is structurally homologous to CaM. While CnB can bind up to four calcium ions, it is constitutively bound to CnA, regardless of the calcium concentration.[12] There are three CaN isoforms: αCaN is found primarily in neurons, βCaN is ubiquitous, and γCaN is largely testes specific.[13] The peptide of the calmodulin binding region of CaN (pCaN) and CaN regulatory domain fragment (RDc) used in this work are from human αCaN. The sequence numbering and use of "CaN" refer to αCaN.

Under resting calcium conditions, CaN is maintained in an inactive state by its autoinhibitory domain (AID) bound to the phophatase catalytic site.[4,13] When calcium levels increase, calmodulin (CaM) binds calcium and then binds to the calmodulin binding region (CaMBR) of CaN, located in the regulatory domain (RD).[14] In the absence of calcium-loaded CaM, the RD is disordered. Binding of CaM to CaN causes an ordering in the RD that removes the AID from CaN's catalytic site, thereby activating the enzyme.[15−17]

In its calcium-loaded form, CaM adopts a somewhat extended structure, with the central linker region remaining flexible, despite the α-helix observed in the crystal structure (Figure 2a).[18−20] Despite this flexibility, CaM is believed to be largely extended in solution.[21] While there are several classes of sequences that CaM can bind, calcium-loaded CaM preferentially binds to basic, amphipathic, α-helical sequences (BAA

Received: April 18, 2014
Revised: August 15, 2014
Published: August 21, 2014

   dx.doi.org/10.1021/bi5004734 | *Biochemistry* 2014, 53, 5779−5790

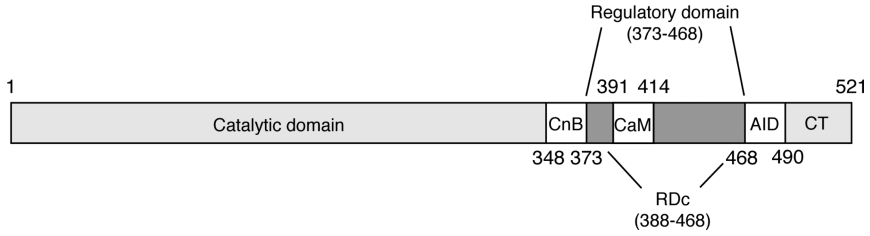

Figure 1. Schematic of human αCnA (CnB not shown). Domain borders are denoted by residue numbering. The pCaN peptide used in this work corresponds to the CaM binding domain (residues 391−414). The location of the residues encompassing the RDc construct (residues 388−468) is noted.

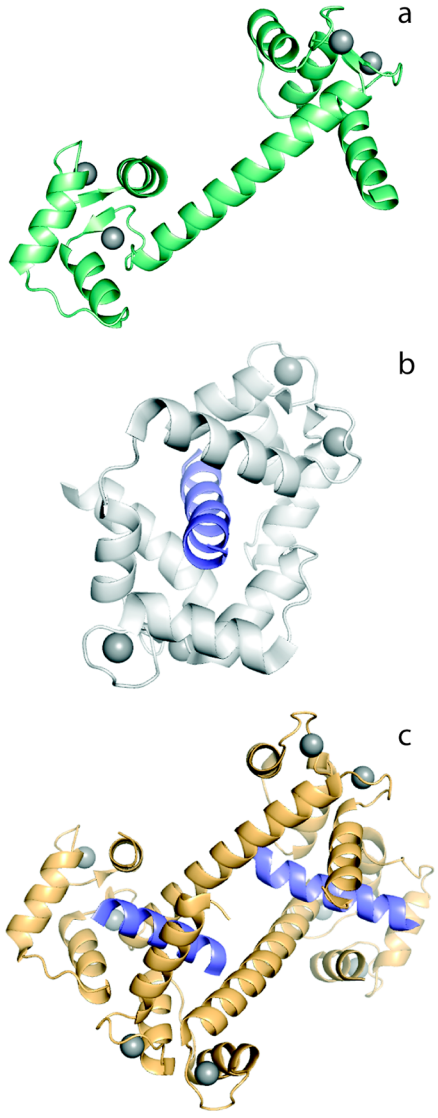

Figure 2. (a) Structure of calcium-loaded CaM (PDB entry 3CLN[18]) (CaM, green; calcium, gray). (b) Structure of CaM bound to smMLCK CaMBR (PDB entry 1CDL[24]) (CaM, pale gray; calcium, gray; CaMBR peptide, blue). (c) Structure (2:2) of CaM bound to pCaN (PDB entry 2R28[28]) (CaM, pale orange; calcium, gray; CaMBR peptide, blue).

sequences).[22,23] Typically, when CaM binds BAA sequences, the CaM central linker region undergoes a change in conformation to allow the two CaM lobes to form a compact ellipsoid wrapped around the target.[22,23] Figure 2b shows CaM bound to its CaMBR from smooth muscle myosin light chain kinase (smMLCK) in this canonical manner.[24] This characteristic binding mode results in its target sequences becoming α-helical. In many cases, such as with CaN, the CaM target sequence is disordered when not bound, but prone to α-helicity.[25,26]

Ye et al. have published crystal structures of CaM bound to pCaN.[27,28] In these structures, the CaM−pCaN complex exists as a 2:2 structure in which the N-terminal lobe of one CaM molecule and the C-terminal lobe of a second CaM molecule interact with a pCaN peptide (Figure 2c). The remaining C- and N-terminal lobes of the two CaM molecules interact with a second pCaN molecule. The interaction occurs such that a pCaN peptide and two CaM lobes interact in an antiparallel fashion. Majava and Kursula have also published a structure of the CaM−pCaN complex in which the stoichiometry is 2:2.[29] Those authors went on to perform small-angle X-ray scattering (SAXS) and size-exclusion chromatography (SEC) on the CaM−pCaN complex. The SAXS data could only be fit to a 1:1 wraparound model, and the SEC data supported a 1:1 complex. The work by both Ye et al. and Majava and Kursula suggests the CaM−pCaN complex can exist as both 1:1 and 2:2 complexes in solution, with a 1:1 complex being the dominant species, and as a 2:2 complex in crystal structures.[27−29] In more recent work, Ye et al. performed SAXS experiments on a larger fragment of CaN that also suggests the complex has a 1:1 stoichiometry in solution.[30]

O'Donnell et al. have performed extensive hydrodynamic work on CaM bound to pCaN from βCaN (pCaNβ).[31] The CaMBR of βCaN differs from that of αCaN by only one residue: V395 in αCaN corresponds to I404 in βCaN. The difference in residue numbering is due to a proline-rich N-terminal extension in CnA of βCaN. Using analytical gel chromatography, sedimentation velocity experiments, and NMR, they could detect only 1:1 CaM−pCaNβ complexes in solution. O'Donnell et al. went on to use NMR experiments to demonstrate binding of CaM to pCaNβ occurs in an antiparallel fashion. The hydrodynamic and NMR data for the CaM−pCaNβ complex put forth by O'Donnell et al. are consistent with a collapsed, wraparound 1:1 structure.[31]

Thus, while solution measurements support a physiological 1:1 complex, no detailed structural information about this state has been obtained. We exhaustively screened for conditions that would allow us to successfully determine the structure of the 1:1 complex. We were able to crystallize the 1:1 complex and determine the structure, demonstrating that it does adopt the canonical wraparound conformation. In addition, we performed analytical size-exclusion chromatography (SEC) on, as well as determined rotational correlation times for, the CaM−RDc complex. The RDc is a construct consisting of the majority of the RD, starting from the CaM binding region and ending at the beginning of the AID (Figure 1), and contains all segments of the RD that we have previously shown become structured upon

dx.doi.org/10.1021/bi5004734 | *Biochemistry* 2014, 53, 5779−5790

CaM binding.[15,16] Our hydrodynamic data indicate that this larger CaM−RDc complex also possesses a 1:1 stoichiometry.

MATERIALS AND METHODS

Proteins, Peptides, and Buffer. Human CaM was expressed from the pETCaMI vector in *Escherichia coli* BL21(DE3) cells (Agilent Technologies, La Jolla, CA) and purified on a 2-(trifluoromethyl)-10-aminopropyl phenothiazine-Sepharose column.[32] The 2-(trifluoromethyl)-10-aminopropyl phenothiazine-Sepharose was synthesized at the Center for Structural Biology Chemistry Core Facility, University of Kentucky.

An *E. coli* codon-optimized gene for the human sequence RD construct (human αCnA residues 373−468) was synthesized by Genscript (Piscataway, NJ) and employed in our previous work.[15,16] This was cloned into the pET303/CT-His vector that adds a C-terminal His_6 tag (Invitrogen, Carlsbad, CA). As described in earlier work, the RDc construct [human αCnA residues 388−468 (Figure 1)] was generated from the RD-pET303/CT-His construct using primers 5′-GGCACCGCGG-CGGCGCGCAAAGAAGTGATTCGC-3′ and 5′-CGCGGT-GCCCGCCATGTCTAGACCTCCTTCTTAAAG-3′ to remove the gene sequence for the residues from the N-terminus of the RD to the beginning of the CaMBR.[16] RDc-pET303/CT-His was cotransformed with pETCaMI for co-expression of RDc and CaM in *E. coli* BL21(DE3) cells. After expression, the RDc was purified on a Ni-NTA column using a urea/thiourea gradient to remove CaM. Clarified RDc-CaM lysate was run over a Ni-NTA column equilibrated in a 7 M urea/thiourea buffer [20 mM Tris (pH 7.5), 200 mM NaCl, 10 mM imidazole, 5 M urea, and 2 M urea]. Five column volumes (CV) of 7 M urea/thiourea buffer were added to the column, and the column was incubated at room temperature, while being being shaken, for 30 min. The urea/thiourea concentration was decreased from 7 to 0.125 M by washing the column six times with 2.5 CV of urea/thiourea buffer that was diluted by half each time. The column was washed with 10 CV of 20 mM Tris (pH 7.5), 200 mM NaCl, and 10 mM imidazole to remove any remaining urea/thiourea. The protein was eluted with 20 mM Tris (pH 7.5), 200 mM NaCl, 2 mM $CaCl_2$, and 250 mM imidazole and further purified with a CaM-Sepharose column. All expressed proteins had their identities confirmed via mass spectrometry. Protein concentrations were determined using absorbance at 280 nm. All reagents used for buffers were obtained from Sigma (St. Louis, MO) and were of the highest purity.

The pCaN peptide (sequence of ARKEVIRNKIRAIGKMA-RVFSVLR) corresponding to the CaM binding region in the RD of αCaN [residues 391−414 (Figure 1)] was purchased from NEO Bioscience (Cambridge, MA). The peptide was purified using reverse-phase high-performance liquid chromatography, and its identity was confirmed using mass spectrometry.

Size-Exclusion Chromatography. Size-exclusion chromatography (SEC) was used to characterize samples of CaM, RDc, and an equimolar mixture of CaM and the RDc. Isocratic elution in 20 mM Tris (pH 7.5), 200 mM NaCl, and 2 mM $CaCl_2$ of 400 μL of a 200 μM solution of each protein was performed through an HR 10/300 Superdex 75 column (GE Life Sciences, Pittsburgh, PA) using an Akta Purifier 10 instrument (GE Life Sciences). The absorbance at 280 nm was used to track protein elution. Gel filtration standards were purchased from Bio-Rad (Hercules, CA). Elution volumes for the standards are listed in Table S1 of the Supporting Information. Protein fractions were analyzed by sodium dodecyl sulfate−polyacrylamide gel electrophoresis (SDS−PAGE) using a Mini-PROTEAN electrophoresis system and precast Any kD TGX gels (Bio-Rad) to determine the protein content of the elution peaks. Bands on the gels were visualized using Coomassie brilliant blue staining.

Calculation of Radii of Hydration. Translational diffusion coefficients, D, of known structures were estimated using HYDROPRO version 10.[33] For each calculation, the solvent density was set at 1.0 g cm^{-3}, the viscosity to 0.009 P, and the temperature to 293 K. The atomic element radius was left at the suggested default value of 2.9 Å, and six equally spaced values of the minibead radius ranging from 1.0 to 2.0 Å were employed. Radii of hydration (R_h) were then estimated from the diffusion coefficients using the Stokes−Einstein equation

$$R_h = \frac{kT}{6\pi\eta D} \quad (1)$$

where k is Boltzmann's constant, T the temperature, and η the solution viscosity.

The radius of gyration of the intrinsically disordered RDc was estimated using

$$R_g = R_0 N^{\upsilon} \quad (2)$$

where N is the number of residues (97 for the RDc, including the additional residues added for purification and concentration determination) and the prefactor R_0 was set to 1.927 Å.[34] The exponent υ can range from 0.33 for a polymer in poor solvent to 0.5 for an ideal solvent to 0.6 for a good solvent. The radius of hydration for the RDc was then estimated from

$$R_h \approx 1.4 R_g \quad (3)$$

an approximate relation derived for highly denatured proteins.[35]

Time-Resolved Fluorescence Spectroscopy. A D3C mutation was made within CaM, and the free cysteine was labeled with Alexa Fluor 488 C_5 maleimide (Life Technologies, Grand Island, NY). Free dye was removed by extensive dialysis. The CaM and Alexa 488 dye concentrations were determined by bicinchoninic acid assay (Thermo-Scientific, Rockford, IL) and the absorbance at 495 nm, respectively. The labeling efficiency of CaM D3C with Alexa 488 was estimated to be ∼99%. This labeled CaM will subsequently be termed CaM488. A pCaN peptide with an additional N-terminal Trp-Gly was synthesized (Atlantic Peptides) for use in fluorescence studies. The RDc construct contains a C-terminal Trp included for concentration determination and fluorescence measurements. All fluorescence samples employed buffers composed of 20 mM Tris (pH 7.5), 200 mM NaCl, 2 mM $CaCl_2$, and 2 mM DTT. Reported measurements are the average of three replicates.

Frequency domain lifetime and anisotropy measurements were taken on an ISS K2 Multifrequency Cross-Correlation Phase and Modulation Fluorometer (ISS, Champaign, IL). All measurements were taken at 20 °C. A 295 nm LED light source (ISS) was used for Trp excitation of 10 μM pCaN or RDc in the presence or absence of equimolar amounts of CaM. Trp was excited using light modulated in frequency from 2 to 220 MHz. *p*-Terphenyl was used as a fluorescence lifetime reference. Trp emissions were passed through a 320 nm long-pass filter (Edmund Optics, Barrington, NJ) before detection 125 nM CaM488 (labeled with Alexa 488) was excited using a 469 nm laser diode (ISS) in the presence or absence of equimolar amounts of pCaN or RDc. CaM488 excitation was modulated from 2 to 150 MHz, and fluorescein was employed as a lifetime reference. Fluorescence emissions from CaM488 passed

dx.doi.org/10.1021/bi5004734 | *Biochemistry* 2014, 53, 5779−5790

through a 530 nm long-pass filter (Edmund Optics) before being detected. Anisotropy decays for both labels were measured under the same conditions and modulation ranges as their respective lifetime measurements.

Lifetime and anisotropy decay data were analyzed using ISS Vinci software (ISS) employing the nonlinear least-squares method. The number of lifetimes and their distributions were determined from fits to either discrete or Lorentzian distributions, with best fits chosen using the lowest χ^2 that gave consistent lifetime data across replicates. The rotational correlation components were estimated using frequency domain anisotropy measurements coupled with the estimated fluorescence lifetime of each fluorophore and analyzed using the ISS Vinci software. Rotational correlation times of our investigated proteins and peptides were compared to those of standards (reference proteins) with established rotational correlation coefficient data (Table S2 of the Supporting Information).[36,37]

Structure Determination. Crystals of the CaM−pCaN complex were grown using hanging-drop vapor-diffusion experiments. Purified and concentrated CaM in 10 mM Tris (pH 7.5) and 2.3 mM $CaCl_2$ was combined with a 1.5-fold molar excess of pCaN to yield a final CaM concentration of 10 mg/mL. This was mixed in a 3:1 protein solution/mother liquor mixture containing 24% PEG 1000 and 20% glycerol in a final volume of 200 nL using a mosquito crystallization robot (TTPLabtech). Crystals were harvested and flash-frozen in liquid nitrogen. Diffraction data to 1.95 Å were collected at the SER-CAT ID-22 beamline of the Advanced Proton Source of Argonne National Laboratory (Argonne, IL) (Table 1). Data were processed using HKL2000.[38]

Table 1. Data Collection and Refinement Statistics

Data Collection	
beamline	APS 22-ID
space group	$C222_1$
wavelength	1.0000
unit cell parameters (Å)	a = 105.499, b = 111.033, c = 39.448
no. of unique reflections	15796
completeness (%)	91.1 (69.6)[a]
resolution (Å)	20.0−1.95 (2.02−1.95)[a]
R_{merge} (%)	9.8 (37.5)[a]
redundancy	5.5 (3.2)[a]
$I/\sigma(I)$	14.4 (3.4)[a]
Refinement	
resolution limits (Å)	20.0−1.95
no. of reflections/no. used to compute R_{free}	14978/801
R (R_{free})	21.5 (24.8)
no. of protein residues	169
no. of solvent molecules	100
no. of calcium molecules	4
Ramachandran[b]	
most favored	98.2
allowed	1.8
disallowed	0
root-mean-square deviation	
bonds (Å)	0.006
angles (deg)	0.972

[a]Values in parentheses are for the highest-resolution shell. [b]Calculated using MolProbity.[54]

An initial molecular replacement solution was obtained using PHASER with calmodulin N-terminal and C-terminal lobes (PDB entry 2W73) as the search model.[39] Clear electron density was observed for the linker region and the pCaN peptide. These regions were built manually. Iterative model building and refinement using COOT[40] with Refmac5[41] and then PHENIX[42] produced a final refined model (Table 1). The atomic coordinates and structure factors have been deposited in the Protein Data Bank (PDB entry 4Q5U). Molecular graphics were prepared using PyMOL.[43] Structure alignments were conducted using PDBeFOLD.[44]

RESULTS

Size-Exclusion Chromatography. Analytical size-exclusion chromatography (SEC) was conducted on CaM, the RDc, and an equimolar mixture of CaM and the RDc to determine the stoichiometry of the complex. SEC traces for each species are shown in Figure 3 along with SDS−PAGE gels for the peak

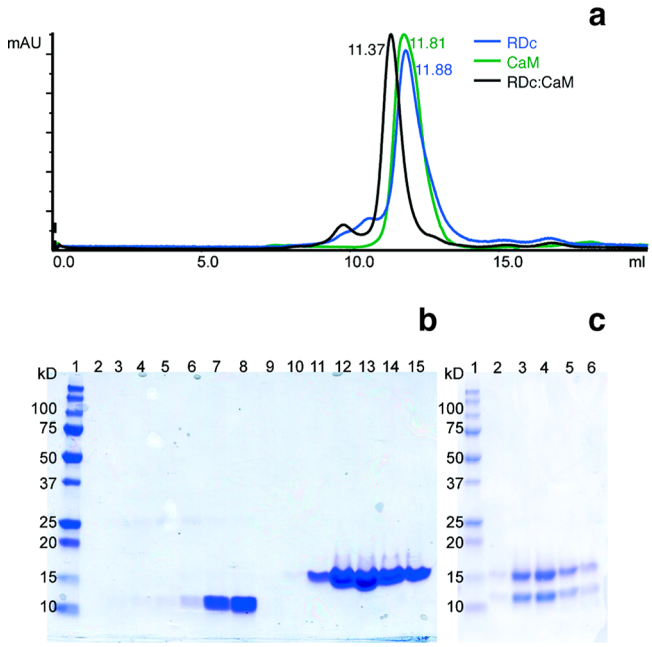

Figure 3. (a) Size-exclusion chromatography traces of CaM alone (green), the RDc alone (blue), and the CaM−RDc complex (gray). (b) SDS−PAGE gel of fractions collected for the SEC peaks for the RDc alone (lanes 2−8) and CaM alone (lanes 9−15). (c) SDS−PAGE gel of fractions collected for the SEC peak for the CaM−RDc complex (lanes 2−6).

elutions. There are low-molecular weight peaks evident for CaM, the RDc, and the CaM/RDc mixture. These smaller molecular species may be degradation products. All three species primarily elute between peaks for the myoglobin (17 kDa) and ovalbumin (44 kDa) standards. These elute at 12.93 and 10.64 mL, respectively (Table S1 of the Supporting Information).

The RDc primarily elutes at 11.88 mL (Figure 3a). There is a shoulder on the peak indicating the presence of a small population of a higher-molecular weight species. Faint bands corresponding to a species with a molecular weight twice that of the RDc can also be seen in the corresponding SDS−PAGE gel (Figure 3b). The RDc construct possesses a N-terminal cysteine used for labeling with fluorophores. This shoulder is then most

dx.doi.org/10.1021/bi5004734 | Biochemistry 2014, 53, 5779−5790

likely due to pairs of molecules that have formed disulfide bonds.

CaM elutes at 11.81 mL, and the CaM/RDc equimolar mixture elutes primarily at 11.37 mL with a second small peak at ~9.5 mL (Figure 3). This latter peak is probably due to two CaM molecules binding to the putative disulfide-bonded RDc pairs observed in the RDc trace. The SDS–PAGE gel for the CaM–RDc mixture indicates that both molecules elute within the one peak around 11.37 mL (Figure 3c).

Rotational Correlation Times. Time-resolved fluorescence spectroscopy was used to determine the rotational correlation times, θ, for CaM488 (CaM D3C labeled with Alexa 488), pCaN, and the RDc, as well as the CaM–pCaN and CaM–RDc complexes (Table S3 of the Supporting Information). Figure 4 is

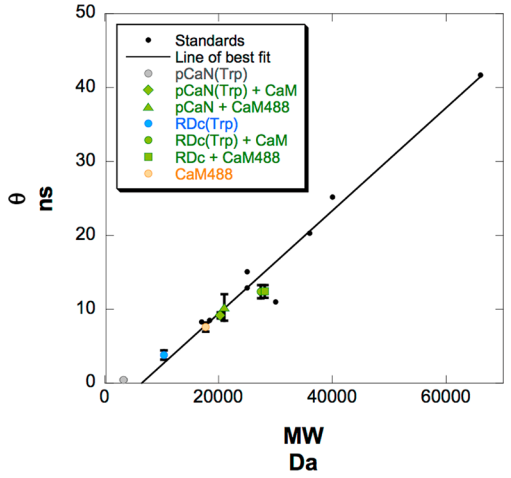

Figure 4. Rotational correlation times (θ) plotted vs molecular weight for eight protein standards, pCaN, the RDc, CaM488, and the CaM–pCaN, CaM488–pCaN, CaM–RDc, and CaM488–RDc complexes.

a plot of previously published rotational correlation times against molecular weight for eight globular proteins we are using as standards (Table S2 of the Supporting Information).[36,37] A line of best fit for to those standards is shown. It should be noted that the line of best fit is given by

$$\theta = 0.0007\mathrm{MW} - 4.5 \quad (r = 0.98) \qquad (4)$$

Clearly negative θ values for low molecular weights would be nonsensical. The negative intercept is likely due to errors in the measurements and/or factors affecting rotation of the proteins that are not related to molecular weight.

Our measured θ values for each species examined here are also plotted in Figure 4. Data are shown for pCaN in the presence of an equimolar amount of CaM determined using fluorescence of Trp on the peptide and for pCaN with an equimolar amount of CaM488 determined using the fluorescence of the Alexa 488 dye conjugated to CaM. Similar data are shown for the RDc with equimolar amounts of CaM and CaM488 (in the presence of DTT). Given the low-picomolar K_d for binding of CaM to its CaMBR from CaN, even at the concentration of 125 nM used for the CaM488 fluorescence measurements, virtually all of the CaM molecules were bound to ligand in these samples.[31,45] In each case, estimated θ values determined using Trp and Alexa 488 are consistent, with the slight differences most likely due to the 721 Da added to the molecular weight of CaM by the Alexa 488 dye. On the basis of the line of best fit derived from the protein standards, a 2:2 CaM–pCaN complex (MW of 39218) would be expected to have a θ value of ~23 ns, and a 2:2 CaM–RDc complex (MW of 54458) would have a θ value of ~33 ns. From our time-resolved fluorescence measurements, the CaM–pCaN and CaM–RDc complexes have rotational correlation times of 9.2 ± 0.4 and 12.4 ± 0.9 ns, respectively, and the CaM488–pCaN and CaM488–RDc complexes times of 10.3 ± 1.8 and 12.4 ± 0.9 ns, respectively (Table S3 of the Supporting Information). These data are consistent with both of the CaM–pCaN and CaM–RDc complexes possessing 1:1 stoichiometry in solution.

Crystal Structure of the CaM–pCaN Complex. The CaM–pCaN complex was crystallized in 10 mM Tris (pH 7.5), 2.3 mM $CaCl_2$ mixed in a 3:1 ratio with 24% PEG 1000, and 20% glycerol, and the structure was determined at a resolution of 1.95 Å. The final structure reveals a 1:1 CaM–pCaN complex, providing the first detailed structural data for the CaM–pCaN complex at this stoichiometry (Figure 5). The

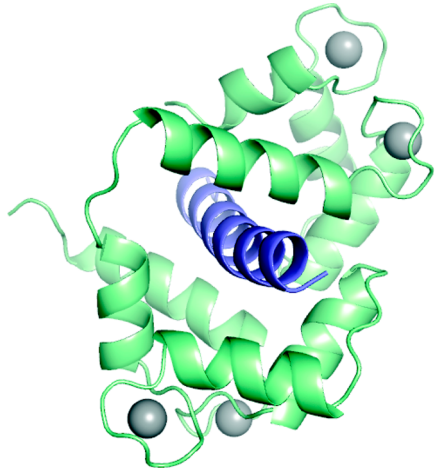

Figure 5. Structure of calcium-loaded CaM bound to pCaN at 1.95 Å resolution. The structure was determined in this work (CaM, green; calcium, gray; CaMBR peptide, blue).

structure displays an antiparallel binding mode: the N-terminal lobe of CaM interacts with the C-terminal end of pCaN, and the C-terminal lobe of CaM interacts with the N-terminal end of pCaN.

The overall conformation of CaM in our structure (Figure 5) resembles that of CaM bound to its CaMBR from smMLCK [PDB entry 1CDL (Figure 2b)],[24] with a root-mean-square deviation (rmsd) of 1.53 Å (Cα–Cα structural alignment of the CaM molecules using PDBeFOLD[44]) indicating a good level of structural similarity. In contrast, the CaM molecules in the 2:2 structure (Figure 2c)[28] more closely resemble those of the extended crystal structure of CaM without substrate bound (Figure 2a; PDB entry 3CLN).[18]

Calcium-loaded CaM has two major hydrophobic pockets that facilitate binding to BAA sequences. These are termed the $FLMM_N$ and $FLMM_C$ pockets, formed by F19, L32, M51, and M71 in the N-terminal lobe of CaM and F92, L105, M124, and M144 in the C-terminal lobe of CaM, respectively.[31,46] M406 of pCaN interacts with the rim of but does not penetrate into the $FLMM_N$ pocket in our CaM–pCaN structure (Figure 6a). I396 and I400 of pCaN interact with M124 and F92 of the $FLMM_C$ pocket but appear to be too distant to be able to bind deeply into the pocket (Figure 7a). Outside of the FLMM pockets, I403 of pCaN interacts with V35 in the N-terminal lobe. A88

dx.doi.org/10.1021/bi5004734 | Biochemistry 2014, 53, 5779–5790

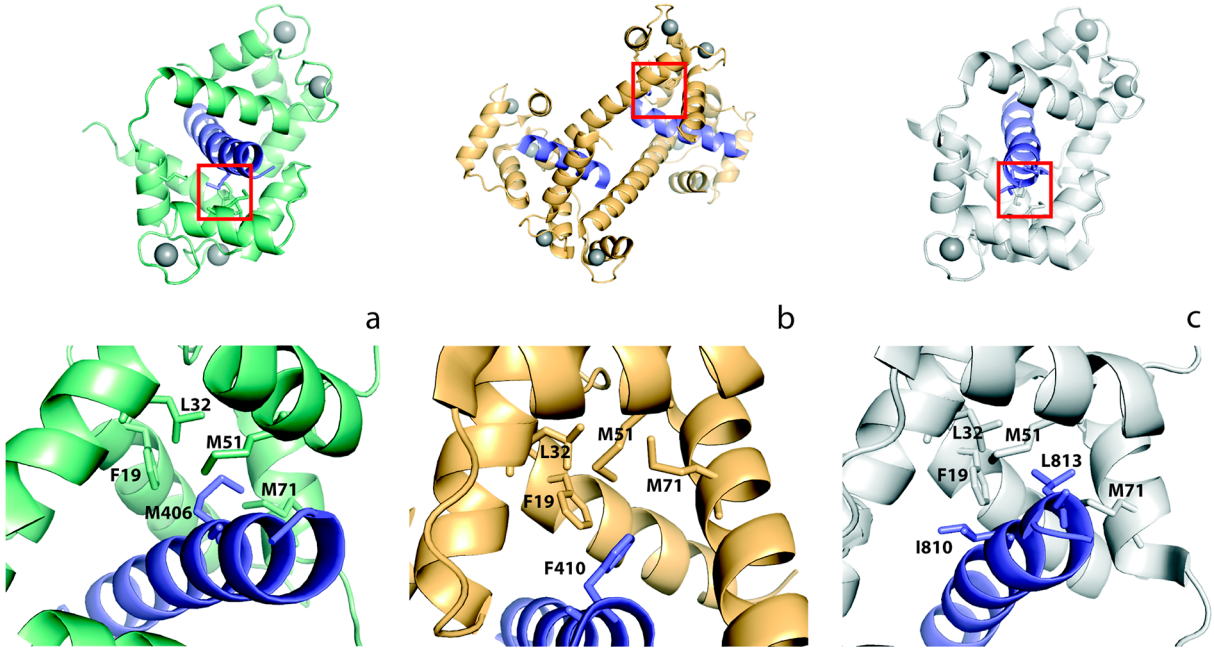

Figure 6. $FLMM_N$ binding pocket interactions. Red boxes indicate the area of interactions in structures, with panels below showing details: (a) 1:1 structure of CaM bound to pCaN that was determined in this work (CaM, green; calcium, gray; CaMBR peptide, blue), (b) 2:2 structure of CaM bound to pCaN (PDB entry 2R28[28]) (CaM, pale orange; calcium, gray; CaMBR peptide, blue), and (c) structure of CaM bound to smMLCK CaMBR (PDB entry 1CDL[24]) (CaM, pale gray; calcium, gray; CaMBR peptide, blue).

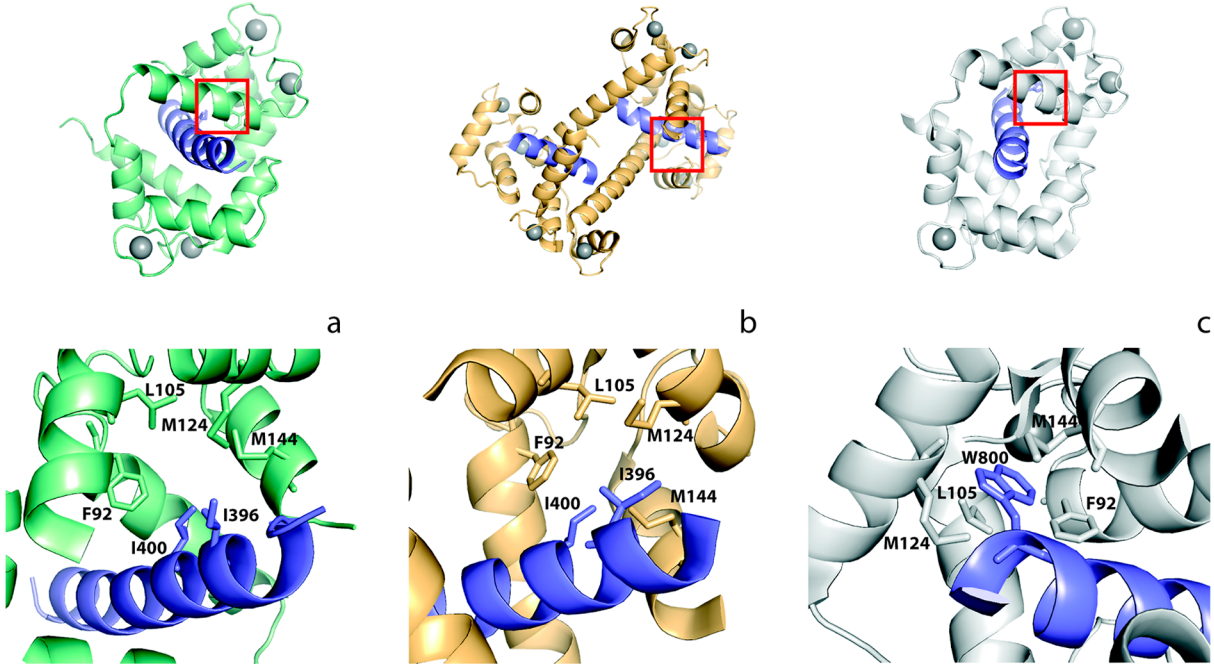

Figure 7. $FLMM_C$ binding pocket interactions. Red boxes indicate the area of interactions in structures, with panels below showing details: (a) 1:1 structure of CaM bound to pCaN that was determined in this work (CaM, green; calcium, gray; CaMBR peptide, blue), (b) 2:2 structure of CaM bound to pCaN (PDB entry 2R28[28]) (CaM, pale orange; calcium, gray; CaMBR peptide, blue), and (c) structure of CaM bound to smMLCK CaMBR (PDB entry 1CDL[24]) (CaM, pale gray; calcium, gray; CaMBR peptide, blue).

and V91, near the C-terminal end of CaM's central linker, also interact with I403. R408 of pCaN forms salt bridges with E83 and D81 of CaM.

DISCUSSION

Hydrodynamic Analyses. Previous hydrodynamic analyses of binding of CaM to CaN have focused on the CaM–pCaN complex.[27−29,31] In each case, the dominant species observed possessed 1:1 stoichiometry. Ye et al. also observed a small, higher-molecular weight population in their experiments that they ascribed to a 2:2 CaM–pCaN complex, consistent with their crystal structures.[27,28] Majava and Kursula performed a SAXS analysis of the CaM–pCaN complex and could fit only a 1:1 structure to the resultant envelope.[29] Recently, Ye et al.

dx.doi.org/10.1021/bi5004734 | *Biochemistry* 2014, 53, 5779−5790

performed a SAXS study on CaM fused to a construct that included CaN RD residues 389−456.[30] These authors found that the resulting envelope was consistent with a 1:1 stoichiometry.

The RDc construct employed in this work differs from that used by Ye et al.[30] in that it is somewhat longer [residues 388−468 (Figure 1)]. We have previously demonstrated that a region between the end of the CaM binding region and the beginning of the AID forms an α-helix.[15,16] Our RDc construct is long enough to ensure we encompass that region.

Analytical SEC is often used to gain estimates of molecular weight. However, the volume at which a protein or complex elutes in such an experiment is more a function of its hydrodynamic size and shape than its molecular weight. For roughly spherical globular proteins such as those used as standards in our SEC experiments (Table S1 of the Supporting Information), the hydrodynamic size is approximately proportional to molecular weight. However, for more elongated molecules such as CaM (Figure 2a) or intrinsically disordered proteins and/or domains such as the RDc, this relationship is at best tenuous. Comparisons of elution volumes and radii of hydration, R_h, are more appropriate.

We have calculated R_h values for CaM, the SEC standards myoglobin and ovalbumin, and 1:1 and 2:2 CaM−pCaN complexes using crystal structures (Table 2). Radii of gyration, R_g, for the RDc were estimated using eq 2 and converted to approximate values of R_h using eq 3. It should be noted that the factor of 1.4 used in eq 3 was derived for highly denatured proteins.[35] Intrinsically disordered proteins are often more collapsed than denatured proteins.[47] Consequently, we have estimated a R_h range for the RDc assuming that it will have an exponent υ in eq 2 somewhere in the range of 0.333−0.5 (Table 2). An exponent of 0.333 is appropriate for a disordered chain in a poor solvent (the chain interacts more favorably with itself than the solvent), and an exponent of 0.5 is appropriate for a chain in a θ solvent (one in which intrachain interactions and chain−solvent interactions are energetically equivalent).[48] Highly denatured proteins obey eq 2 power law with an exponent closer to 0.6.

Table 2. Estimated Radii of Hydration (R_h) for Each Protein Species Examined Here and Two of the Standard Proteins Used in the SEC Measurements

species	PDB entry	MW (Da)[a]	R_h (Å)
CaM	3CLN	16838	23.9
1:1 CaM−pCaN	4Q5U	19632	22.2
2:2 CaM−pCaN	2R28	39218	29.0
myoglobin	4DC8	16894	21.1
ovalbumin	1OVA	42881	28.8
RDc	−	10392	12.2−24.9

[a]Estimated from the residues visible in each crystal structure. Full MW for RDc used.

CaM has been estimated to occupy an extended conformation such as that in Figure 2a ∼70% of the time, so its estimated R_h of 23.9 Å is expected to be greater than that of the SEC standard of very similar molecular weight myoglobin (Table 2).[21] This is consistent with CaM eluting via SEC at a volume smaller than that of myoglobin. The estimated range of R_h for the RDc (12.2−24.9 Å) is very broad, starting well below the R_h of the heavier myoglobin and extending beyond that for CaM. Given that the RDc elutes at a volume slightly larger than that of CaM (Figure 3), we conclude that the RDc is somewhat compact, but not nearly as compact as would be expected for a chain in a poor solvent. Like many intrinsically disordered regions, the sequence of the RDc is enriched with polar residues and poor in hydrophobes.[15,16,49] Aqueous buffer would be a poor solvent for hydrophobic residues, and a better one for polar residues. An enrichment with polar residues, and in particular charged residues, will lead to somewhat more expanded disordered ensembles.[47]

When compared to the R_h estimates in Table 2, our SEC data (Figure 3) are consistent with the CaM−RDc complex possessing a stoichiometry of 1:1. The structure of the 1:1 CaM−pCaN complex obtained in this work yields an estimated R_h of 22.2 Å. This should be considered an underestimate for the CaM−RDc complex because the RDc is 97 residues in length (including the His_6 tag, and residues added for concentration determination and fluorophore tagging purposes) as opposed to the 24-residue pCaN peptide. The CaM−RDc complex elutes at 11.37 mL, before CaM at 11.81 mL (Figure 3), but well after the ovalbumin standard at 10.64 mL (Table S1 of the Supporting Information). This suggests that the R_h of the CaM−RDc complex is significantly less than the value of 28.8 Å estimated for ovalbumin. Note that the 2:2 CaM−pCaN complex has an estimated R_h of 29.0 Å (Table 2), which is similar to that of ovalbumin but is an underestimate for a 2:2 CaM−RDc complex.

The rotational correlation times, θ, determined using time-resolved fluorescence provide support that both CaM−pCaN and CaM−RDc complexes are 1:1 complexes (Figure 4). As noted above, the estimated θ values of the CaM−RDc and CaM488−RDc of the complexes are approximately half that which would be expected were they 2:2 complexes. However, the θ values determined for all the species examined here fall relatively close to the line of best fit for the protein standards (Figure 4 and Table S2 of the Supporting Information). These observations are most consistent with the RDc and CaM488 being monomeric and CaM−RDc and CaM488−RDc complexes existing as 1:1 complexes in solution.

Taken together, the data from our SEC and rotational correlation time measurements support a 1:1 stoichiometry for the CaM−:RDc complex. Furthermore, our estimated θ values for the CaM−pCaN and CaM488−pCaN complexes are also supportive of 1:1 stoichiometries. These observations are in good agreement with the hydrodynamic work of Ye et al., Majava and Kursula, and O'Donnell et al. on CaM−pCaN complexes.[27−29,31]

Structural Comparison to the 1:1 CaM−smMLCK Complex. Our crystallographic structure determination of the CaM−pCaN complex reveals a 1:1 stoichiometry (Figure 5). In our structure, the complex has adopted the canonical wrap-around conformation typically observed for CaM bound to BAA sequences (e.g., Figure 2b). The 2.4 Å structure of CaM bound to its binding region from smMLCK determined by Meador et al. [PDB entry 1CDL (Figure 2b)] is often considered an archetype of CaM bound to a BAA sequence.[24] The superimposition of the CaM molecules from our structure (PDB entry 4Q5U) with the structure of Meador et al. is shown in Figure 8. The PDBeFOLD server returned a rmsd of 1.53 Å for this Cα−Cα superimposition.[44] Interestingly, when our structure is used as the query in a PDBeFOLD search for similar structures in the entire PDB, entry 1QS7 is returned as the best match with a rmsd of 1.19 Å. This is an unpublished 1.8 Å

dx.doi.org/10.1021/bi5004734 | Biochemistry 2014, 53, 5779−5790

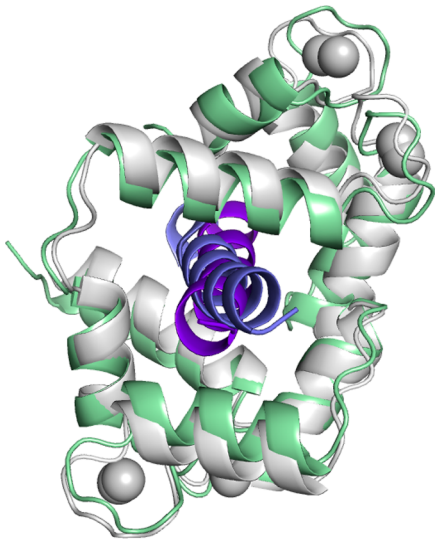

Figure 8. Structure of the CaM−pCaN complex determined in this work (PDB entry 4Q5U; CaM, pale green; pCaN, blue) superimposed onto the structure of CaM bound to the smMLCK peptide (PDB entry 1CDL;[24] CaM, white; smMLCK, purple). Calcium ions are depicted as gray spheres.

resolution crystal structure of CaM bound to the smMLCK peptide.

The CaM molecules in Figure 8 adopt very similar structures, although the two peptides differ somewhat in conformation. The peptide in each structure is bound in an antiparallel manner with their N-terminal region interacting with the C-terminal lobe of CaM. As would be expected, the differences in peptide conformation are due to their sequence differences. As illustrated in Figure 7, I396 and I400 from pCaN in our structure interact with the outside of the $FLMM_C$ pocket, whereas W800 from the smMLCK peptide penetrates deeply into the pocket. At the C-termini of the peptides, M406 from pCaN interacts with residues from but does not penetrate into the $FLMM_N$ pocket, whereas L813 from smMLCK is nestled into that pocket. The net result is that the terminal regions of the smMLCK peptide appear to be bound more closely to the CaM lobes than the terminal regions of pCaN. In fact, the two peptides bury similar amounts of surface area when they are bound by CaM (1577 Å^2 for pCaN and 1537 Å^2 for the smMLCK peptide). Despite this, CaM binds the smMLCK peptide with a K_d in the nanomolar range, whereas pCaN is bound much more tightly with a low-picomolar K_d.[31,45,50,51] This in part is likely due to burial of hydrophobic surface area. The hydrophobic residues in pCaN (defined here as those with aliphatic side chains, methionine, and the aromatics) bury a total of 817 Å^2, whereas the smMLCK peptide buries 652 Å^2.

Ataman et al. analyzed the structures of 16 complexes of CaM bound to BAA peptides.[46] These authors determined that each of the residues in the $FLMM_N$ pocket, F19, L32, M51, and M71, is in direct contact with bound peptide residues in ≥75% of the structures examined. In our structure, residues from pCaN are in contact with M51 and M71, seemingly consistent with this observation (Figure 6). Ataman et al. also found that three of the residues making up the $FLMM_C$ pocket, F92, M124, and M144, made direct contacts with all of the BAA peptides, and the fourth residue within the pocket, L105, contacted 15 of the 16 peptides.[46] In contrast, in our structure, the pCaN peptide appears to make contact with just F92 and M124 of the CaM $FLMM_C$ pocket (Figure 7). Most notably, however, in contrast to the peptides in the BAA structures examined by Ataman et al.,[46] residues from pCaN do not significantly penetrate into the FLMM pockets but rather interact with what would be the outer edges of these pockets. This is illustrated in Figure 6a where the side chain of pCaN residue M406 is pointed away from the $FLMM_N$ pocket, and in Figure 7a where the side chains of pCaN residues I396 and I400 are not close enough to penetrate the $FLMM_C$ pocket. These observations provide evidence that the CaM binding surfaces, which include the FLMM pockets, possess a remarkable level of plasticity, which can be inferred from the large number of sequences CaM is known to bind.[23]

Structural Comparison to the Previous 2:2 CaM−pCaN Complexes. The crystal structures of the previous three CaM−

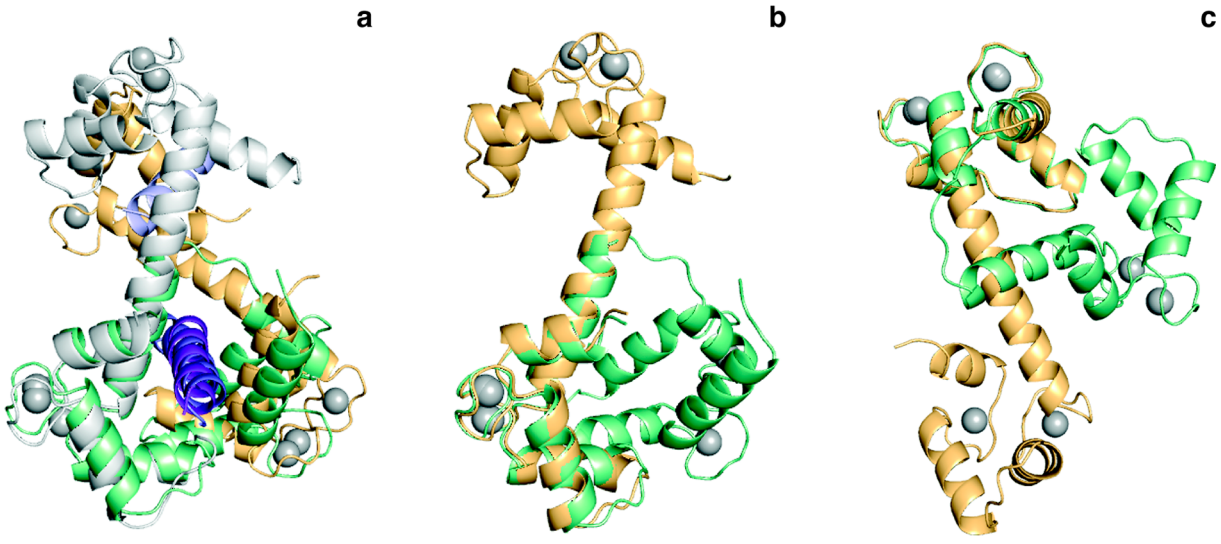

Figure 9. Structure of the 1:1 CaM−pCaN complex (PDB entry 4Q5U; CaM, pale green; pCaN, blue) superimposed on the structure of a 2:2 CaM−pCaN complex (PDB entry 2R28[28]). (A) N-Terminal lobe of the 1:1 structure superimposed on that of chain A (pale orange) in the 2:2 structure, and the C-terminal lobe superimposed on that of chain B (white). (b) N-Terminal lobe of the 1:1 structure superimposed on that of chain A (pale orange) from the 2:2 structure. (c) C-Terminal lobe of the 1:1 structure superimposed on that of chain A (pale orange) from the 2:2 structure.

dx.doi.org/10.1021/bi5004734 | *Biochemistry* 2014, 53, 5779−5790

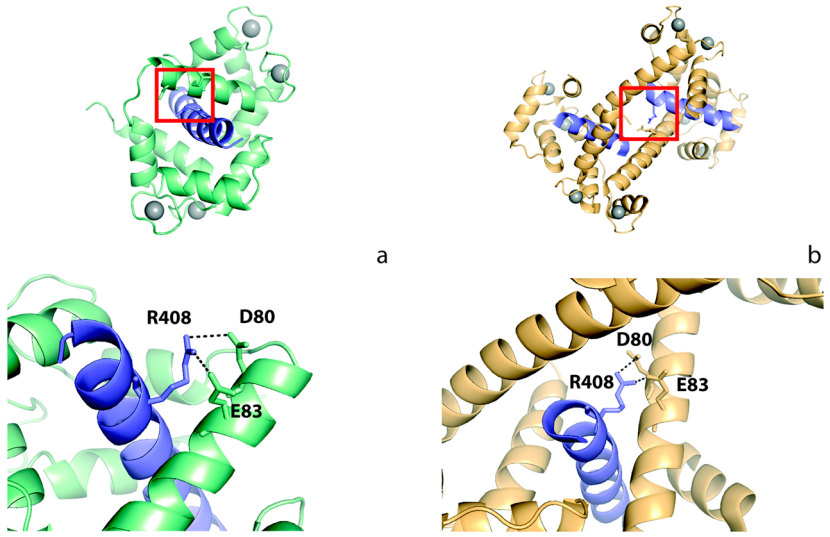

Figure 10. Salt bridge interaction between R408 of pCaN and D80 and E83 of CaM. Red boxes indicate the area of interactions in structures, with panels below showing details: (a) 1:1 structure of CaM bound to pCaN that was determined in this work (CaM, green; calcium, gray; CaMBR peptide, blue) and (b) 2:2 structure of CaM bound to pCaN (PDB entry 2R28[28]) (CaM, pale orange; calcium, gray; CaMBR peptide, blue).

pCaN complexes have each revealed CaM bound to pCaN with a 2:2 stoichiometry.[27−29] Because all of the existing 2:2 structures are very similar, all comparisons with our structure will be made relative to the 2R28 structure. In these 2:2 structures, the pCaN peptide is bound in a pseudoantiparallel manner, with the N-terminal region of each peptide bound to the C-terminal lobe of a CaM molecule and the peptide C-terminal regions bound to N-terminal lobes. The conformations of the CaM molecules in the 2:2 structures, however, are in a more extended form (Figure 2c) than the CaM in our 1:1 complex (Figure 5). Indeed, our 1:1 structure cannot be aligned with either of the individual CaM molecules from the 2:2 structure (PDB entry 2R28) in a reasonable manner. A superimposition of our structure using both CaM chains in the 2:2 structure is shown in Figure 9a. In this structural alignment, the N-terminal lobe of our structure has been aligned with the N-terminal lobe of CaM chain A in the 2:2 structure and the C-terminal lobe with the C-terminal lobe of CaM chain B. This yielded an rmsd of 3.16 Å. In fact, with rmsd's of 2.1 and 2.2 Å, the CaM molecules in the 2:2 structure are more similar to the peptide-free crystal structure of CaM than to our structure. From visual inspection of Figure 9a, it would appear that the C-terminal lobes are better aligned than the N-terminal lobes.

We superimposed the N-terminal lobe (specifically residues 5−70) of our structure with the N-terminal lobe of CaM chain A of the 2:2 structure (Figure 9b). The rmsd for aligning these 66 residues was 1.13 Å. Superimposing the C-terminal lobe of our structure (residues 78−147) with that of CaM chain A from the 2:2 structure yielded an rmsd of 0.88 Å (Figure 9c). Therefore, while the overall conformations of the CaM molecules in our structure and the 2:2 structures are dissimilar, the calcium-binding lobes are very alike.

There are similarities between the CaM−pCaN intermolecular interactions in our 1:1 structure and those in the previously reported 2:2 structures.[28] I396 and I400 of pCaN interact with M124 and F92 of the $FLMM_C$ pocket of CaM, respectively, in all structures. I403 of pCaN interacts with A88, V91, and V35 in CaM in all of the structures, as well. Finally, R408 of pCaN forms salt bridges with E83 and D81 of CaM in all structures (Figure 10). Surprisingly, these R408−E83 and R408−D81 interactions occur between pCaN and the linker helix of CaM that is one long helix in the 2:2 complexes but is more looplike in our 1:1 complex.

Despite these similarities, the significantly different conformation of CaM in our 1:1 complex results in unique interactions or loss of interactions as compared to the 2:2 complex. In addition to the salt bridges between R408 of pCaN, and E83 and D81 of CaM, in our structure we observe two CaM−pCaN salt bridges not observed in the 2:2 structures. These are an interaction between R392 of pCaN and E14 of CaM and one between R414 and E47. Notably, neither R392 nor R414 of pCaN is seen in the 2:2 structure reported by Ye et al.[28]

In their 2:2 crystal structure, Ye et al. observe interactions between CaM's central linker helix and pCaN: M72 and M76 of CaM interact with V409 and F410 of the pCaN peptide.[28] In our 1:1 structure, we do not observe the interactions between M72 and M76 of CaM and V409 and F410 of pCaN. The shortest distance is from M76 to V409, and that distance is ∼10 Å; F410 is on the opposite side of the pCaN helix from the two CaM methionines.

Our 1:1 structure and the 2:2 structures share similar interactions between CaM and pCaN at the $FLMM_C$ pocket (Figure 7) as noted above but have very different interactions at the $FLMM_N$ pocket (Figure 6). In BAA sequences with one aromatic residue, the aromatic is usually buried in the $FLMM_C$ pocket, and in sequences with more than one aromatic residue, one usually resides in each FLMM pocket.[31,46] This is illustrated by the structure of CaM bound to its CaMBR from smMLCK; W800 of smMLCK is buried within the $FLMM_C$ pocket (Figure 7c).[24] Instead of an aromatic in either FLMM pocket, our 1:1 CaM−pCaN complex reveals M406 of pCaN contacting all four of the residues making up, but not penetrating deeply into, the $FLMM_N$ pocket (Figure 6a). Similar to the 2:2 structures, I396 and I400 of pCaN interact with M124 and F92 of $FLMM_C$, but no residues extend deeply into the pocket.

pCaN possesses a single aromatic residue, F410. In our 1:1 CaM−pCaN complex, F410 is not buried in either FLMM pocket but instead ring-stacks with P43 of CaM (Figure 11). For

dx.doi.org/10.1021/bi5004734 | *Biochemistry* 2014, 53, 5779−5790

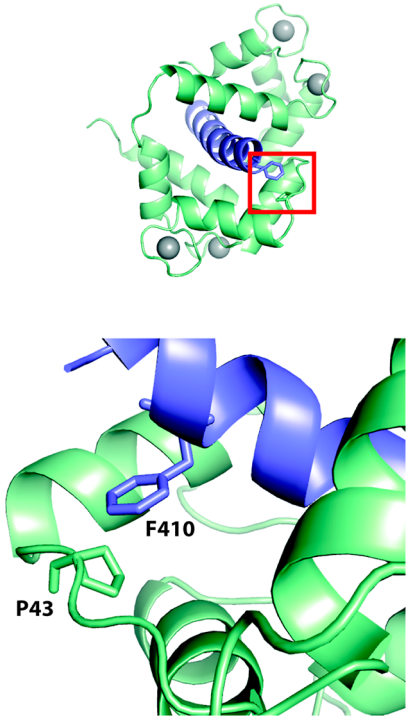

Figure 11. Ring stacking interaction between F410 of pCaN and P43 of CaM in the 1:1 structure of CaM bound to the pCaN structure determined in this work (CaM, green; calcium, gray; CaMBR peptide, blue).

example, CE1 of F410 is ~3.7 Å from both CB and CG of P43. An interaction between F410 in pCaN and P43 in CaM is supported by NMR work performed by O'Donnell et al.[31] They observed an intermolecular NOE between F419 of pCaNβ (equivalent to F410) and P43 in CaM. Notably, they did not record any NOEs between F419 of pCaNβ and residues within the $FLMM_N$ pocket. This observation, combined with other data described in this section, links the 1:1 stoichiometry we observe in our structure with that observed in solution studies.

There are other marked differences between the structure of the CaM–pCaN complex determined here (Figure 5) and the 2:2 structures determined previously (Figure 2c).[27−29] In the 2:2 structure, electron density for only 15 residues of one pCaN peptide (molecule C, I396–F410) and 19 of the other (molecule D, K393–S411) was observed in the 2R28 structure, whereas all 24 residues (A391–R414) were identified in our structure. As a result, the peptides in the 2:2 structure appear to bury just 1297 and 1318 $Å^2$ of solvent accessible surface area (chains C and D, respectively), whereas pCaN in our structure has 1577 $Å^2$ buried, more consistent with the very tight binding measured by O'Donnell et al.[31]

Why Ye et al. and Majava and Kursula observed 2:2 complexes whereas we obtained a 1:1 structure for the CaM–pCaN complex is not clear.[27−29] In all of the structures, the CaM sequence used was identical. The first 2:2 structure, determined by Ye et al., consisted of a pCaN peptide slightly longer than that employed here, with one additional alanine at the N-terminus, fused to the C-terminus of CaM via a five-glycine linker.[27] The second structure reported by Ye et al. employed the same peptide, but in this case not fused to CaM.[28] Majava and Kursula used a shorter 17-residue peptide corresponding to CaN residues 395–411.[29] One could argue that this last 2:2 structure arose as a result of this shorter peptide, but that would be inconsistent with the structures of Ye et al. that employed a peptide slightly longer than our pCaN.[27,28]

Differences in resolution, and thus interpretation of the electron density, also do not appear to be contributing factors. In their initial publication, Ye et al. obtained two crystal forms, space groups *P*321 and *C*2, that diffracted to 2.6 and 2.17 Å, respectively.[27] In their second publication, they obtained two similar crystal forms.[28] These diffracted to ~3 and 2.1 Å, respectively. The latter data set was used to produce the 2R28 structure via molecular replacement using their structures obtained from the CaM–pCaN fusion construct (PDB entries 2F2P and 2F2O). Majava and Kursula obtained a single crystal type that diffracted to 1.45 Å (space group $P2_1$, PDB entry 2W73).[29] Their structure was obtained via molecular replacement using a CaM–pCaN fusion structure. Our structure, also obtained from a single crystal type, has a resolution of 1.95 Å and was determined via molecular replacement using the N- and C-terminal lobes of CaM from one chain in the 2W73 2:2 structure. Given the final resolutions of each of these structures, they can be considered reliable.

The most likely explanation for previous authors obtaining 2:2 complexes in their structures versus our 1:1 complex would be differences in crystallization conditions. The crystals used for 2:2 structures were obtained under a variety of conditions. The CaM–pCaN fusion structures determined by Ye et al. used crystals grown in the presence of 29% (w/v) PEG 2K, 0.2 M ammonium sulfate, and 0.1 M malonic acid at pH 4.5 (space group *P*321) and 0.1 M citrate at pH 4.5 (*C*2).[27] Their next structures were obtained from crystals grown in the presence of 0.1 M sodium acetate, 0.2 M magnesium formate, and 20% (w/v) PEG 3350 at pH 4.5 (space group not reported) and 0.2 M ammonium phosphate, 0.1 M citrate, and 20% (w/v) PEG 3350 at pH 4.5 (*C*2).[28] Majava and Kursula obtained their single crystal form (space group $P2_1$) in the presence of 30% (w/v) PEG 400, 200 mM potassium chloride, and 100 mM Tris-HCl at pH 8.5.[29] Finally, our structure was obtained from crystals grown in the presence of 24% (w/v) PEG 1000 and 20% glycerol (space group *C*222). The most noticeable difference is the lack of salts in our crystallization mother liquor. How this might result in the observed structural differences is not at all clear. This is especially puzzling given that CaM binds to pCaN very tightly (K_d ~ 1 pM), resulting in what should be an extremely stable complex.[31] Indeed, we observed in previous work that this complex is not thermally denatured even at a temperature of 95 °C.[16]

CONCLUSIONS

From our hydrodynamic studies performed on CaM–RDc complexes, and the crystal structure we determined of the CaM–pCaN fusion protein, we conclude that both exist primarily as a 1:1 complex. Solution and hydrodynamic studies by Majava and Kursula, O'Donnell et al., and Ye et al. have also shown that the dominant form of the CaM–pCaN fusion protein in solution is the 1:1 species.[29−31] Our crystal structure demonstrates that CaM binds to the CaMBR from CaN in the collapsed, wraparound form observed for many CaM–CaMBR complexes (Figure 5). The collapsed, wraparound structure is consistent with the very tight (K_d ~ 1–28 pM) binding of CaM to CaN.[31,45] Such a structure is also consistent with the observation that the RD from calcium-loaded CaN is disordered.[15] The binding of CaM in this form would be greatly facilitated by the CaMBR being in a disordered state as opposed to being part of a folded, globular structure. Our

dx.doi.org/10.1021/bi5004734 | *Biochemistry* 2014, 53, 5779–5790

hydrodynamic data using the longer RDc construct demonstrate that an increase in the length of the pCaN sequence to encompass the majority of CaN's RD does not alter the stoichiometry of the complex. Coupled with our previous observations that the RD undergoes a large-scale folding upon CaM binding,[15,16] the data presented here indicate that a single CaM molecule is required to bind to a single CaN heterodimer to remove the AID from the active site and activate the phosphatase.

It has been suggested that the disordered nature of the CaN RD is an intermediate state between low-calcium and high-calcium, CaM-bound states in which the RD is folded.[17] The hypothesis is that the disordered state facilitates rapid binding of CaM. Quintana et al. have determined that CaM does bind CaN quite rapidly with an on rate of $\sim 5 \times 10^7$ M^{-1} s^{-1}.[45] This on rate is in the range for binding of CaM to CaN via what is known as the "fly casting" mechanism.[52,53] In fly casting, the rate of binding is rapid because one of the binding partners is disordered and thus has a larger capture radius. A 1:1 stoichiometry for the CaM−CaN complex, making the association a bimolecular reaction (treating the CaN heterodimer as a single entity), would facilitate this, leading to rapid activation of the phosphatase. A 2:2 stoichiometry would likely promote slower activation because four, and perhaps minimally three, proteins would need to associate. Rapid activation of CaN is important for it to fulfill its function in signaling networks, particularly, for example, in neuronal signaling.

■ ASSOCIATED CONTENT

Supporting Information

Size-exclusion chromatography standards run on the HR 10/300 Superdex 75 column (Table S1), rotational correlation time protein standards (Table S2), and estimated rotational correlation times from time-resolved fluorescence (Table S3). This material is available free of charge via the Internet at http://pubs.acs.org.

■ AUTHOR INFORMATION

Corresponding Author

*E-mail: trevor.creamer@uky.edu. Phone: (859) 323-6037. Fax: (859) 257-2283.

Funding

T.B.D. was supported by a Predoctoral Fellowship from the American Heart Association (11PRE7020001). This work was supported by grants from the National Science Foundation (MCB-0843551) and the Kentucky Science and Engineering Foundation (KSEF-148-502-08-227) to T.P.C. The University of Kentucky Center for Structural Biology Chemistry Core Facility is supported in part by funds from National Institutes of Health National Center for Research Resources Grant P20 RR020171 (Principal Investigator, Professor Louis B. Hersh).

Notes

The authors declare no competing financial interest.

■ ACKNOWLEDGMENTS

We thank Professor Anthony Persechini of the University of Missouri at Kansas City (Kansas City, MO) for providing the pETCaMI expression vector.

■ ABBREVIATIONS

CaN, calcineurin; CaM, calmodulin; CnA, calcineurin's A chain; CnB, calcineurin's B chain; CaMBR, calmodulin binding region; RD, calcineurin's regulatory domain; AID, calcineurin's autoinhibitory domain; MLCK, myosin light chain kinase; NFAT, nuclear factor activating T-cells; pCaN, peptide corresponding to the calmodulin binding region in calcineurin; SEC, size-exclusion chromatography; PDB, Protein Data Bank.

■ REFERENCES

(1) Wang, J. H., and Desai, R. (1976) A brain protein and its effect on the Ca^{2+}- and protein modulator-activated cyclic nucleotide phosphodiesterase. *Biochem. Biophys. Res. Commun. 72*, 926−932.

(2) Watterson, D. M., and Vanaman, T. C. (1976) Affinity chromatography purification of a cyclic nucleotide phosphodiesterase using immobilized modulator protein, a troponin C-like protein from brain. *Biochem. Biophys. Res. Commun. 73*, 40−46.

(3) Klee, C. B., and Krinks, M. H. (1978) Purification of cyclic 3″,5″-nucleotide phosphodiesterase inhibitory protein by affinity chromatography on activator protein coupled to Sepharose. *Biochemistry 17*, 120−126.

(4) Rusnak, F., and Mertz, P. (2000) Calcineurin: Form and function. *Physiol. Rev. 80*, 1483−1521.

(5) Ermak, G., Morgan, T. E., and Davies, K. J. (2001) Chronic overexpression of the calcineurin inhibitory gene DSCR1 (Adapt78) is associated with Alzheimer's disease. *J. Biol. Chem. 276*, 38787−38794.

(6) Ermak, G., and Davies, K. J. A. (2013) Chronic high levels of the RCAN1-1 protein may promote neurodegeneration and Alzheimer disease. *Free Radical Biol. Med. 62*, 47−51.

(7) Hoeffer, C. A., Dey, A., Sachan, N., Wong, H., Patterson, R. J., Shelton, J. M., Richardson, J. A., Klann, E., and Rothermel, B. A. (2007) The Down syndrome critical region protein RCAN1 regulates long-term potentiation and memory via inhibition of phosphatase signaling. *J. Neurosci. 27*, 13161−13172.

(8) Chakraborti, S., Das, S., Kar, P., Ghosh, B., Samanta, K., Kolley, S., Ghosh, S., Roy, S., and Chakraborti, T. (2007) Calcium signaling phenomena in heart diseases: A perspective. *Mol. Cell. Biochem. 298*, 1−40.

(9) Vega, R. B., Bassel-Duby, R., and Olson, E. N. (2003) Control of cardiac growth and function by calcineurin signaling. *J. Biol. Chem. 278*, 36981−36984.

(10) Rao, A., Luo, C., and Hogan, P. G. (1997) Transcription factors of the NFAT family: Regulation and function. *Annu. Rev. Immunol. 15*, 707−747.

(11) Hubbard, M. J., and Klee, C. B. (1989) Functional domain structure of calcineurin A: Mapping by limited proteolysis. *Biochemistry 28*, 1868−1874.

(12) Stemmer, P. M., and Klee, C. B. (1994) Dual calcium ion regulation of calcineurin by calmodulin and calcineurin B. *Biochemistry 33*, 6859−6866.

(13) Klee, C. B., Ren, H., and Wang, X. (1998) Regulation of the calmodulin-stimulated protein phosphatase, calcineurin. *J. Biol. Chem. 273*, 13367−13370.

(14) Yang, S. A., and Klee, C. B. (2000) Low affinity Ca^{2+}-binding sites of calcineurin B mediate conformational changes in calcineurin A. *Biochemistry 39*, 16147−16154.

(15) Rumi-Masante, J., Rusinga, F. I., Lester, T. E., Dunlap, T. B., Williams, T. D., Dunker, A. K., Weis, D. D., and Creamer, T. P. (2012) Structural basis for activation of calcineurin by calmodulin. *J. Mol. Biol. 415*, 307−317.

(16) Dunlap, T. B., Cook, E. C., Rumi-Masante, J., Arvin, H. G., Lester, T. E., and Creamer, T. P. (2013) The distal helix in the regulatory domain of calcineurin is important for domain stability and enzyme function. *Biochemistry 52*, 8643−8651.

(17) Creamer, T. P. (2013) Transient disorder: Calcineurin as an example. *Intrinsically Disordered Proteins 1*, e26412.

(18) Babu, Y. S., Bugg, C. E., and Cook, W. J. (1988) Structure of calmodulin refined at 2.2 Å resolution. *J. Mol. Biol. 204*, 191−204.

(19) Zhang, M., Tanaka, T., and Ikura, M. (1995) Calcium-induced conformational transition revealed by the solution structure of apo calmodulin. *Nat. Struct. Biol. 2*, 758−767.

(20) Kuboniwa, H., Tjandra, N., Grzesiek, S., Ren, H., Klee, C. B., and Bax, A. (1995) Solution structure of calcium-free calmodulin. *Nat. Struct. Biol. 2*, 768−776.
(21) Sorensen, B. R., and Shea, M. A. (1996) Calcium binding decreases the Stokes radius of calmodulin and mutants R74A, R90A, and R90G. *Biophys. J. 71*, 3407−3420.
(22) Crivici, A., and Ikura, M. (1995) Molecular and structural basis of target recognition by calmodulin. *Annu. Rev. Biophys. Biomol. Struct. 24*, 85−116.
(23) Yap, K. L., Kim, J., Truong, K., Sherman, M., Yuan, T., and Ikura, M. (2000) Calmodulin target database. *J. Struct. Funct. Genomics 1*, 8−14.
(24) Meador, W. E., Means, A. R., and Quiocho, F. A. (1992) Target enzyme recognition by calmodulin: 2.4 Å structure of a calmodulin-peptide complex. *Science 257*, 1251−1255.
(25) Radivojac, P., Vucetic, S., O'Connor, T. R., Uversky, V. N., Obradovic, Z., and Dunker, A. K. (2006) Calmodulin signaling: Analysis and prediction of a disorder-dependent molecular recognition. *Proteins 63*, 398−410.
(26) Dunlap, T. B., Kirk, J. M., Pena, E. A., Yoder, M. S., and Creamer, T. P. (2013) Thermodynamics of binding by calmodulin correlates with target peptide α-helical propensity. *Proteins 81*, 607−612.
(27) Ye, Q., Li, X., Wong, A., Wei, Q., and Jia, Z. (2006) Structure of calmodulin bound to a calcineurin peptide: A new way of making an old binding mode. *Biochemistry 45*, 738−745.
(28) Ye, Q., Wang, H., Zheng, J., Wei, Q., and Jia, Z. (2008) The complex structure of calmodulin bound to a calcineurin peptide. *Proteins 73*, 19−27.
(29) Majava, V., and Kursula, P. (2009) Domain swapping and different oligomeric states for the complex between calmodulin and the calmodulin-binding domain of calcineurin a. *PLoS One 4*, e5402.
(30) Ye, Q., Feng, Y., Yin, Y., Faucher, F., Currie, M. A., Rahman, M. N., Jin, J., Li, S., Wei, Q., and Jia, Z. (2013) Structural basis of calcineurin activation by calmodulin. *Cell. Signalling 25*, 2661−2667.
(31) O'Donnell, S., Yu, L., Fowler, C. A., and Shea, M. A. (2011) Recognition of β-calcineurin by the domains of calmodulin: Thermodynamic and structural evidence for distinct roles. *Proteins 79*, 765−786.
(32) Charbonneau, H., Hice, R., Hart, R. C., and Cormier, M. J. (1983) Purification of calmodulin by Ca^{2+}-dependent affinity chromatography. *Methods Enzymol. 102*, 17−39.
(33) Ortega, A., Amorós, D., and García de la Torre, J. (2011) Prediction of hydrodynamic and other solution properties of rigid proteins from atomic- and residue-level models. *Biophys. J. 101*, 892−898.
(34) Kohn, J. E., Millett, I. S., Jacob, J., Zagrovic, B., Dillon, T. M., Cingel, N., Dothager, R. S., Seifert, S., Thiyagarajan, P., Sosnick, T. R., Hasan, M. Z., Pande, V. S., Ruczinski, I., Doniach, S., and Plaxco, K. W. (2004) Random-coil behavior and the dimensions of chemically unfolded proteins. *Proc. Natl. Acad. Sci. U.S.A. 101*, 12491−12496.
(35) Receveur-Bréchot, V., and Durand, D. (2012) How Random are Intrinsically Disordered Proteins? A Small Angle Scattering Perspective. *Curr. Protein Pept. Sci. 13*, 55−75.
(36) Yguerabide, J., Epstein, H. F., and Stryer, L. (1970) Segmental Flexibility in an Antibody Molecule. *J. Mol. Biol. 51*, 573−590.
(37) Lakowicz, J. R. (2006) *Principles of fluorescence spectroscopy*, Springer Verlag, Berlin.
(38) Otwinowski, Z., and Minor, W. (1997) Processing of X-ray diffraction data. *Methods Enzymol. 276*, 307−326.
(39) McCoy, A. J., Grosse-Kunstleve, R. W., Adams, P. D., Winn, M. D., Storoni, L. C., and Read, R. J. (2007) Phaser crystallographic software. *J. Appl. Crystallogr. 40*, 658−674.
(40) Emsley, P., Lohkamp, B., Scott, W. G., and Cowtan, K. (2010) Features and development of Coot. *Acta Crystallogr. D66*, 486−501.
(41) Murshudov, G. N., Skubák, P., Lebedev, A. A., Pannu, N. S., Steiner, R. A., Nicholls, R. A., Winn, M. D., Long, F., and Vagin, A. A. (2011) REFMAC5 for the refinement of macromolecular crystal structures. *Acta Crystallogr. D67*, 355−367.
(42) Zwart, P. H., Afonine, P. V., Grosse-Kunstleve, R. W., Hung, L.-W., Ioerger, T. R., McCoy, A. J., McKee, E., Moriarty, N. W., Read, R. J., Sacchettini, J. C., Sauter, N. K., Storoni, L. C., Terwilliger, T. C., and Adams, P. D. (2008) Automated structure solution with the PHENIX suite. *Methods Mol. Biol. 426*, 419−435.
(43) *The PyMOL Molecular Graphics System*, version 1.3 (2010) Schrödinger LLC, Portland, OR.
(44) Krissinel, E., and Henrick, K. (2004) Secondary-structure matching (SSM), a new tool for fast protein structure alignment in three dimensions. *Acta Crystallogr. D60*, 2256−2268.
(45) Quintana, A. R., Wang, D., Forbes, J. E., and Neal Waxham, M. (2005) Kinetics of calmodulin binding to calcineurin. *Biochem. Biophys. Res. Commun. 334*, 674−680.
(46) Ataman, Z. A., Gakhar, L., Sorensen, B. R., Hell, J. W., and Shea, M. A. (2007) The NMDA receptor NR1 C1 region bound to calmodulin: Structural insights into functional differences between homologous domains. *Structure 15*, 1603−1617.
(47) Das, R. K., and Pappu, R. V. (2013) Conformations of intrinsically disordered proteins are influenced by linear sequence distributions of oppositely charged residues. *Proc. Natl. Acad. Sci. U.S.A. 110*, 13392−13397.
(48) Tanford, C., Kawahara, K., and Lapanje, S. (1966) Proteins in 6-M guanidine hydrochloride. Demonstration of random coil behavior. *J. Biol. Chem. 241*, 1921−1923.
(49) Radivojac, P., Iakoucheva, L. M., Oldfield, C. J., Obradovic, Z., Uversky, V. N., and Dunker, A. K. (2007) Intrinsic disorder and functional proteomics. *Biophys. J. 92*, 1439−1456.
(50) Wintrode, P. L., and Privalov, P. L. (1997) Energetics of target peptide recognition by calmodulin: A calorimetric study. *J. Mol. Biol. 266*, 1050−1062.
(51) Brokx, R. D., Lopez, M. M., Vogel, H. J., and Makhatadze, G. I. (2001) Energetics of target peptide binding by calmodulin reveals different modes of binding. *J. Biol. Chem. 276*, 14083−14091.
(52) Shoemaker, B. A., Portman, J. J., and Wolynes, P. G. (2000) Speeding molecular recognition by using the folding funnel: The fly-casting mechanism. *Proc. Natl. Acad. Sci. U.S.A. 97*, 8868−8873.
(53) Kiefhaber, T., Bachmann, A., and Jensen, K. S. (2012) Dynamics and mechanisms of coupled protein folding and binding reactions. *Curr. Opin. Struct. Biol. 22*, 21−29.
(54) Chen, V. B., Arendall, W. B., Headd, J. J., Keedy, D. A., Immormino, R. M., Kapral, G. J., Murray, L. W., Richardson, J. S., and Richardson, D. C. (2010) MolProbity: All-atom structure validation for macromolecular crystallography. *Acta Crystallogr. D66*, 12−21.